(This is a sample cover image for this issue. The actual cover is not yet available at this time.)

International Journal of Engineering Science 62 (2013) 48–55

Contents lists available at SciVerse ScienceDirect

International Journal of Engineering Science

journal homepage: www.elsevier.com/locate/ijengsci

On the longitudinal wave along a functionally graded magneto-electro-elastic rod

Chun-Xia Xue [a,*], Ernian Pan [b,*]

[a] Department of Mechanics, College of Science, North University of China, Taiyuan 030051, PR China
[b] Department of Civil Engineering, University of Akron, Akron, OH 44325, USA

ARTICLE INFO

Article history:
Received 30 December 2011
Received in revised form 14 August 2012
Accepted 19 August 2012

Keywords:
Functional gradient material
Magneto-electro-elastic
Long circular rod
Longitudinal wave
Effective Young's modulus
Effective Poisson's ratio

ABSTRACT

We consider a functionally graded magneto-electro-elastic rod made of piezoelectric $BaTiO_3$ and piezomagnetic $CoFe_2O_4$. The materials properties are assumed to vary exponentially along the rod direction. We derive the one-dimensional wave-motion equation for the functionally graded magneto-electro-elastic rod. Furthermore, for this one-dimensional problem, we demonstrate the phase velocity and frequency spectrum, and discuss the important influence of the gradient factor as well as material coupling on the wave features. We also calculate and compare the effective Young's modulus and effective Poisson's ratio in the $BaTiO_3$- $CoFe_2O_4$ composite rod made of different volume fractions of $BaTiO_3$, showing clearly the important effect of the material coupling on these parameters.

1. Introduction

The functionally graded material (FGM) structure has attracted wide and increasing attentions to scientists and engineers (i.e., Rubio, Silva, & Paulino, 2009). FGM plays an essential role in most advanced integrated systems for vibration control and health monitoring. Recently, owing to its three phase coupling, the magneto-electro-elastic (MEE) material is being studied extensively (i.e., Bayrashev, Robbins, & Ziaie, 2004; Wu & Huang, 2000). Structures made of such materials could be applied to convert energy from one type to the other, and therefore, could be utilized for energy harvesting.

Pan (2001) and Pan and Heyliger (2002) derived the three-dimensional exact closed-form solution for anisotropic MEE plates under simply supported edge conditions for both static and vibration cases. Bhangale and Ganesan (2006) investigated the static deformation of the corresponding functionally graded magneto-electro-elastic (FG-MEE) plates using a semi-analytical finite element method. The bending problem of the anisotropic FG-MEE beams subjected to polynomial loads was analyzed by Huang, Ding, and Chen (2007).

Wave propagation in piezoelectric beam and plate structures based on the classical and refined models was studied by Wang and coworkers (Quek & Wang, 2000; Wang & Quek, 2000). Based on both the classical and Mindlin–Herrmann rod models, Wang and Varadan (2002) further investigated the longitudinal wave propagation in rods with a coated piezoelectric layer. Recently, using the Legendre orthogonal polynomial series expansion approach, Yu and Wu (2009) studied the circumferential wave in FG-MEE cylindrical curved plates and obtained the electric and magnetic potential distributions at different wave numbers. Zhang and Chen (2010) discussed the characteristics of the torsional wave propagating in a piezoelectric hollow cylinder with unattached electrodes.

* Corresponding authors. Tel.: +1 330 972 6739; fax: +1 330 972 6020.
E-mail addresses: xuechunxia@nuc.edu.cn (C.-X. Xue), pan2@uakron.edu (E. Pan).

0020-7225/$ - see front matter © 2012 Elsevier Ltd. All rights reserved.
http://dx.doi.org/10.1016/j.ijengsci.2012.08.004

In this paper, we study the wave propagation in an FG-MEE long and circular rod made of piezoelectric $BaTiO_3$ and piezomagnetic $CoFe_2O_4$. The one-dimensional longitudinal wave equation is derived and solved in Section 2. Numerical results on the effect of the gradient factor as well as material coupling on the wave features are presented in Section 3, and conclusions are drawn in Section 4.

2. Longitudinal wave in a functionally graded magneto-electro-elastic rod

2.1. Basic equations

For a circular rod of radius R made of transversely isotropic FG-MEE material, we assume that the z-axis is normal to the plane of material isotropy (Fig. 1), and that the material coefficients vary exponentially along the longitudinal z-direction of the rod in a unified manner as (i.e., Bhangale & Ganesan, 2006; Pan & Han, 2005; Zhao & Chen, 2010):

$$c_{ij} = c_{ij}^0 e^{\alpha z},\ \ e_{ij} = e_{ij}^0 e^{\alpha z},\ \ q_{ij} = q_{ij}^0 e^{\alpha z},\ \ \kappa_{ij} = \kappa_{ij}^0 e^{\alpha z},\ \ d_{ij} = d_{ij}^0 e^{\alpha z},\ \ \mu_{ij} = \mu_{ij}^0 e^{\alpha z},\ \ \rho = \rho^0 e^{\alpha z} \tag{1}$$

where c_{ij}, e_{ij}, q_{ij}, κ_{ij}, d_{ij}, μ_{ij} and ρ are, respectively, the elastic, piezoelectric, piezomagnetic, dielectric, magnetoelectric, magnetic coefficients and the density of the material. The superscript 0 is used to denote the constant factor of the material property, and α is the gradient index of the material. We point out that complicated variation of the material properties could be approximated by the piecewise exponential function variation, and thus the study presented in this paper is fundamentally useful. In the cylindrical coordinate system (r, θ, z), z is along the rod direction, i.e., the wave propagation direction, and $\theta \in [0,2\pi]$, $0 \leqslant r \leqslant R$. The constitutive relations in the cylindrical coordinate system are

$$\begin{aligned}
\sigma_r &= c_{11}\varepsilon_r + c_{12}\varepsilon_\theta + c_{13}\varepsilon_z - e_{31}E_z - q_{31}H_z \\
\sigma_\theta &= c_{12}\varepsilon_r + c_{11}\varepsilon_\theta + c_{13}\varepsilon_z - e_{31}E_z - q_{31}H_z \\
\sigma_z &= c_{13}\varepsilon_r + c_{13}\varepsilon_\theta + c_{33}\varepsilon_z - e_{33}E_z - q_{33}H_z \\
\tau_{rz} &= c_{44}\gamma_{rz} - e_{15}E_r - q_{15}H_r \\
\tau_{\theta z} &= c_{44}\gamma_{\theta z} - e_{15}E_\theta - q_{15}H_\theta \\
\tau_{r\theta} &= c_{66}\gamma_{r\theta}
\end{aligned} \tag{2}$$

$$\begin{aligned}
D_r &= e_{15}\gamma_{rz} + \kappa_{11}E_r + d_{11}H_r \\
D_\theta &= e_{15}\gamma_{\theta z} + \kappa_{11}E_\theta + d_{11}H_\theta \\
D_z &= e_{31}\varepsilon_r + e_{31}\varepsilon_\theta + e_{33}\varepsilon_z + \kappa_{33}E_z + d_{33}H_z
\end{aligned} \tag{3}$$

$$\begin{aligned}
B_r &= q_{15}\gamma_{rz} + d_{11}E_r + \mu_{11}H_r \\
B_\theta &= q_{15}\gamma_{\theta z} + d_{11}E_\theta + \mu_{11}H_\theta \\
B_z &= q_{31}\varepsilon_r + q_{31}\varepsilon_\theta + q_{33}\varepsilon_z + d_{33}E_z + \mu_{33}H_z
\end{aligned} \tag{4}$$

where σ_i and τ_{ij} are the normal and shear stresses; ε_i and γ_{ij} are the normal and shear strains; E_i, H_i, D_i, and B_i are, respectively, the electric field, magnetic field, electric displacements, and magnetic inductions. For a transversely isotropic material, the relation $c_{11} = c_{12} + 2c_{66}$ holds.

In the absence of body forces with further free electric/magnetic body source, the equations of motion in the long rod are

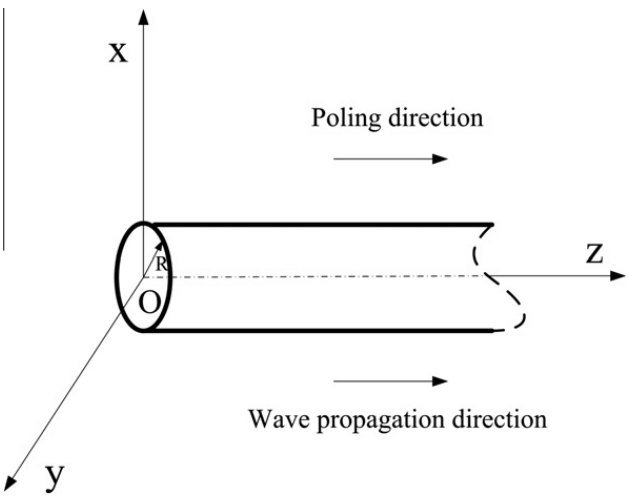

Fig. 1. An FG-MEE circular rod of radius R with wave propagating in the longitudinal z-direction, which is also the poling direction of the material.

$$\begin{aligned}
&\frac{\partial\sigma_r}{\partial r}+\frac{\partial\tau_{r\theta}}{r\partial\theta}+\frac{\partial\tau_{rz}}{\partial z}+\frac{\sigma_r-\sigma_\theta}{r}=\rho\frac{\partial^2 u_r}{\partial t^2}\\
&\frac{\partial\tau_{r\theta}}{\partial r}+\frac{\partial\sigma_\theta}{r\partial\theta}+\frac{\partial\tau_{\theta z}}{\partial z}+\frac{2\tau_{r\theta}}{r}=\rho\frac{\partial^2 u_\theta}{\partial t^2}\\
&\frac{\partial\tau_{rz}}{\partial r}+\frac{\partial\tau_{\theta z}}{r\partial\theta}+\frac{\partial\sigma_z}{\partial z}+\frac{\tau_{rz}}{r}=\rho\frac{\partial^2 u_z}{\partial t^2}
\end{aligned} \tag{5}$$

$$\frac{\partial D_r}{\partial r}+\frac{\partial D_\theta}{r\partial\theta}+\frac{\partial D_z}{\partial z}+\frac{D_r}{r}=0 \tag{6}$$

$$\frac{\partial B_r}{\partial r}+\frac{\partial B_\theta}{r\partial\theta}+\frac{\partial B_z}{\partial z}+\frac{D_r}{r}=0 \tag{7}$$

where u_r, u_θ, and u_z are, respectively, the mechanical displacements in r-, θ-, and z-directions.

The elastic strain–displacement relations can be expressed as:

$$\begin{aligned}
&\varepsilon_r=\frac{\partial u_r}{\partial r},\ \ \varepsilon_\theta=\frac{\partial u_\theta}{r\partial\theta}+\frac{u_r}{r},\ \ \varepsilon_z=\frac{\partial u_z}{\partial r}\\
&\gamma_{r\theta}=\frac{\partial u_r}{r\partial\theta}+\frac{\partial u_\theta}{\partial r}-\frac{u_\theta}{r},\ \ \gamma_{\theta z}=\frac{\partial u_z}{r\partial\theta}+\frac{\partial u_\theta}{\partial z},\ \ \gamma_{rz}=\frac{\partial u_z}{\partial r}+\frac{\partial u_r}{\partial z}
\end{aligned} \tag{8}$$

In this study, the following assumptions are made: (1) the cross section of the rod remains plane before and after the deformation; (2) the lateral surface of the rod is axial symmetry, implying that $u_\theta = 0$ and $\partial/\partial\theta = 0$, which gives further $\gamma_{\theta z} = 0$, $E_\theta = 0$, and $H_\theta = 0$; (3) in order to consider the Poisson's effect, we assume (Xue, Pan, & Zhang, 2011; Zhang & Liu, 2008) that the gradient of the longitudinal displacement u_z and the radial displacement u_r is connected by $u_r = -v_{\text{eff}} r\partial u_z/\partial z$ where v_{eff} is the effective Poisson's ratio to be determined later.

Thus, for the one-dimensional long rod made of FG-MEE, the field quantities depend only on the z-coordinate in the rod direction. Furthermore, the extended tractions on the lateral boundary ($r = R$) of the rod should be zero. Consequently, one could assume that in the whole problem domain $\sigma_r = 0$, $\tau_{rz} = 0$, $\tau_{r\theta} = 0$, $D_r = 0$, $B_r = 0$. From these and the symmetric deformation assumption above, we obtain the following relations:

$$\gamma_{r\theta}=\gamma_{\theta z}=0, E_r=E_\theta=0, H_r=H_\theta=0, D_\theta=B_\theta=0,, \tag{9}$$

$$\varepsilon_\theta=\frac{e_{31}E_z+q_{31}H_z-c_{11}\varepsilon_r-c_{13}\varepsilon_z}{c_{12}} \tag{10}$$

According to the Maxwell's equations, the E- and H-fields in z-direction are related to the electric potential ϕ and magnetic potential ψ by the following relations:

$$E_z=-\frac{\partial\phi}{\partial z},\quad H_z=-\frac{\partial\psi}{\partial z} \tag{11}$$

Furthermore, the equations of motion are reduced to

$$\frac{\sigma_\theta}{r}=v_{\text{eff}}\rho r\frac{\partial^3 u_z}{\partial t^2\partial z},\ \ \frac{\partial\sigma_z}{\partial z}=\rho\frac{\partial^2 u_z}{\partial t^2} \tag{12a, b}$$

$$\frac{\partial D_z}{\partial z}=0,\ \ \frac{\partial B_z}{\partial z}=0 \tag{12c, d}$$

2.2. Longitudinal wave equations

First, in terms of u_z, ϕ and ψ, Eqs. (12a–d) become

$$A_1\frac{\partial\phi}{\partial z}+A_2\frac{\partial\psi}{\partial z}+(A_4-A_3v_{\text{eff}})\frac{\partial u_z}{\partial z}=v_{\text{eff}}\rho r^2\frac{\partial^3 u_z}{\partial t^2\partial z} \tag{13}$$

$$\frac{\partial}{\partial z}[B_1\frac{\partial\phi}{\partial z}+B_2\frac{\partial\psi}{\partial z}+(B_3-A_4v_{\text{eff}})\frac{\partial u_z}{\partial z}]=\rho\frac{\partial^2 u_z}{\partial t^2} \tag{14}$$

$$\frac{\partial}{\partial z}\left[C_1\frac{\partial\phi}{\partial z}+C_2\frac{\partial\psi}{\partial z}+(A_1v_{\text{eff}}-B_1)\frac{\partial u_z}{\partial z}\right]=0 \tag{15}$$

$$\frac{\partial}{\partial z}\left[C_2\frac{\partial\phi}{\partial z}+D_1\frac{\partial\psi}{\partial z}+(A_2v_{\text{eff}}-B_2)\frac{\partial u_z}{\partial z}\right]=0 \tag{16}$$

where

$$A_1 = \left(1 - \frac{c_{12}^0}{c_{11}^0}\right) e_{31}^0 e^{\alpha z} \equiv A_1^0 e^{\alpha z}, \;\; A_2 = \left(1 - \frac{c_{12}^0}{c_{11}^0}\right) q_{31}^0 e^{\alpha z} \equiv A_2^0 e^{\alpha z}$$
$$A_3 = \left(c_{11}^0 - \frac{c_{12}^0 c_{12}^0}{c_{11}^0}\right) e^{\alpha z} \equiv A_3^0 e^{\alpha z}, \;\; A_4 = c_{13}^0 \left(1 - \frac{c_{12}^0}{c_{11}^0}\right) e^{\alpha z} \equiv A_4^0 e^{\alpha z} \tag{17a}$$

$$B_1 = \left(e_{33}^0 - \frac{c_{13}^0}{c_{11}^0} e_{31}^0\right) e^{\alpha z} \equiv B_1^0 e^{\alpha z}, \;\; B_2 = \left(q_{33}^0 - \frac{c_{13}^0}{c_{11}^0} q_{31}^0\right) e^{\alpha z} \equiv B_2^0 e^{\alpha z}$$
$$B_3 = \left(c_{33}^0 - \frac{c_{13}^0 c_{13}^0}{c_{11}^0}\right) e^{\alpha z} \equiv B_3^0 e^{\alpha z} \tag{17b}$$

$$C_1 = \left(\frac{e_{31}^0}{c_{11}^0} e_{31}^0 + \kappa_{33}^0\right) e^{\alpha z} \equiv C_1^0 e^{\alpha z}, \;\; C_2 = \left(\frac{e_{31}^0}{c_{11}^0} q_{31}^0 + d_{33}^0\right) e^{\alpha z} \equiv C_2^0 e^{\alpha z}$$
$$D_1 = \left(\frac{q_{31}^0}{c_{11}^0} q_{31}^0 + \mu_{33}^0\right) e^{\alpha z} \equiv D_1^0 e^{\alpha z} \tag{17c}$$

We now take the derivative of Eq. (13) with respect to z to obtain

$$A_1^0 \frac{\partial^2 \phi}{\partial z^2} + A_2^0 \frac{\partial^2 \psi}{\partial z^2} + \left(A_4^0 - A_3^0 v_{\text{eff}}\right) \frac{\partial^2 u_z}{\partial z^2} = \rho^0 v_{\text{eff}} r^2 \frac{\partial^4 u_z}{\partial t^2 \partial z^2} \tag{18}$$

Integrating both sides of Eq. (18) over the cross-section of the rod, we arrive at

$$A_1^0 \frac{\partial^2 \phi}{\partial z^2} + A_2^0 \frac{\partial^2 \psi}{\partial z^2} + \left(A_4^0 - A_3^0 v_{\text{eff}}\right) \frac{\partial^2 u_z}{\partial z^2} = \frac{1}{2} \rho^0 v_{\text{eff}} R^2 \frac{\partial^4 u_z}{\partial t^2 \partial z^2} \tag{19a}$$

From Eqs. (14)–(16), we can get

$$\alpha \left[B_1^0 \frac{\partial \phi}{\partial z} + B_2^0 \frac{\partial \psi}{\partial z} + \left(B_3^0 - A_4^0 v_{\text{eff}}\right) \frac{\partial u_z}{\partial z}\right] + B_1^0 \frac{\partial^2 \phi}{\partial z^2} + B_2^0 \frac{\partial^2 \psi}{\partial z^2} + \left(B_3^0 - A_4^0 v_{\text{eff}}\right) \frac{\partial^2 u_z}{\partial z^2} = \rho^0 \frac{\partial^2 u_z}{\partial t^2} \tag{19b}$$

$$\alpha \left[C_1^0 \frac{\partial \phi}{\partial z} + C_2^0 \frac{\partial \psi}{\partial z} + \left(A_1^0 v_{\text{eff}} - B_1^0\right) \frac{\partial u_z}{\partial z}\right] + C_1^0 \frac{\partial^2 \phi}{\partial z^2} + C_2^0 \frac{\partial^2 \psi}{\partial z^2} + \left(A_1^0 v_{\text{eff}} - B_1^0\right) \frac{\partial^2 u_z}{\partial z^2} = 0 \tag{19c}$$

$$\alpha \left[C_2^0 \frac{\partial \phi}{\partial z} + D_1^0 \frac{\partial \psi}{\partial z} + \left(A_2^0 v_{\text{eff}} - B_2^0\right) \frac{\partial u_z}{\partial z}\right] + C_2^0 \frac{\partial^2 \phi}{\partial z^2} + D_2^0 \frac{\partial^2 \psi}{\partial z^2} + \left(A_2^0 v_{\text{eff}} - B_2^0\right) \frac{\partial^2 u_z}{\partial z^2} = 0 \tag{19d}$$

Eqs. (19a–d) form the wave equations in terms of u_z, ϕ and ψ. For the wave propagating along the rod z-direction, we can assume the solutions as:

$$u_z(z,t) = U e^{\text{ik(z-ct)}}, \phi(z,t) = \Phi e^{\text{ik(z-ct)}}, \psi(z,t) = \Psi e^{\text{ik(z-ct)}} \tag{20}$$

where $i = \sqrt{(-1)}$ is the imaginary unit, k the wave number, c the phase velocity of the wave. Furthermore, U, Φ and Ψ are the amplitudes of the displacement, electric potential and magnetic potential, respectively. Substituting Eq. (20) into Eqs. (19a-d) yields

$$\begin{aligned}&\left[A_1^0 A_1^0 D_1^0 - A_1^0 A_2^0 C_2^0 + A_2^0 A_2^0 C_1^0 - A_1^0 A_2^0 C_2^0 - A_3^0 C_2^0 C_2^0 + A_3^0 C_1^0 D_1^0 - \frac{1}{2} \rho^0 R^2 k^2 c^2 \left(C_1^0 D_1^0 - C_2^0 C_2^0\right)\right] v_{\text{eff}} + A_1^0 C_2^0 B_2^0 - A_1^0 B_1^0 D_1^0 \\ &- C_1^0 A_2^0 B_2^0 + C_2^0 A_2^0 B_1^0 + C_2^0 A_4^0 C_2^0 - C_1^0 A_4^0 D_1^0 \\ &= 0\end{aligned} \tag{21a}$$

$$(1 - \alpha i/k)\left(B_3^0 - C_{\text{mee}}\right) = \rho^0 c^2 \tag{21b}$$

where

$$C_{\text{mee}} = \frac{\left(A_1^0 D_1^0 B_1^0 - A_2^0 C_2^0 B_1^0 - A_1^0 B_2^0 C_2^0 + A_2^0 C_1^0 B_2^0 + A_4^0 C_1^0 D_1^0 - A_4^0 C_2^0 C_2^0\right) v_{\text{eff}}}{C_1^0 D_1^0 - C_2^0 C_2^0} + \frac{2 B_1^0 C_2^0 B_2^0 - B_1^0 D_1^0 B_1^0 - B_2^0 C_1^0 B_2^0}{C_1^0 D_1^0 - C_2^0 C_2^0} \tag{22}$$

is defined as the MEE coupling factor, and the effective Poisson's ratio v_{eff} is

$$v_{\text{eff}} = -\frac{\varepsilon_\theta}{\varepsilon_z} = \frac{q_{33}^0 q_{31}^0 + \mu_{33}^0 c_{13}^0 + \left(d_{33}^0 q_{31}^0 - e_{31}^0 \mu_{33}^0\right)\left(e_{33}^0 \mu_{33}^0 - q_{33}^0 d_{33}^0\right) \Big/ \left(d_{33}^0 d_{33}^0 - \kappa_{33}^0 \mu_{33}^0\right)}{2 q_{31}^0 q_{31}^0 + \mu_{33}^0 \left(c_{11}^0 + c_{12}^0\right) + 2\left(d_{33}^0 q_{31}^0 - e_{31}^0 \mu_{33}^0\right)\left(e_{31}^0 \mu_{33}^0 - q_{31}^0 d_{33}^0\right) \Big/ \left(d_{33}^0 d_{33}^0 - \kappa_{33}^0 \mu_{33}^0\right)} \tag{23}$$

While Eq. (21a) gives a simple expression of the circular frequency ω ($\equiv kc$) as a function of the material property as well as the radius of the rod, Eq. (21b) solves the longitudinal wave velocity in terms of the material gradient factor α in the FG-MEE rod as

$$c = \sqrt{(B_3^0 - C_{\text{mee}})(1 - \alpha i/k)/\rho^0} \tag{24}$$

Or using the relation $\omega = kc$, we have

$$k^2 - \alpha k i = \frac{\rho^0 \omega^2}{B_3^0 - C_{\text{mee}}} \equiv \Omega^2 \tag{25}$$

It is clear from Eq. (25) that the wave number k is in general complex and can be assumed as $k = m + ib$, with m and b being real numbers. Furthermore, since the wave behaviors are similar for u_z, ϕ and ψ (see Eq. (20)), we only discuss those associated with the elastic displacement u_z. Substituting Eq. (25) into the first expression in Eq. (20), we have

$$\begin{aligned} u_z(z,t) &= U\exp[i(kz - \omega t)] = U\exp\left[i\sqrt{\left(B_3^0 - C_{\text{mee}}\right)/\rho^0}\left(k\Big/\sqrt{\left(B_3^0 - C_{\text{mee}}\right)/\rho^0}z - \Omega t\right)\right] \\ &= U\exp\left[i\sqrt{(B_3^0 - C_{\text{mee}})/\rho^0}(Kz - \Omega t)\right] \end{aligned} \tag{26}$$

where $K = k/\sqrt{(B_3^0 - C_{\text{mee}})/\rho^0}$. Depending on the k value, we have the following three cases:

Case 1: $4\Omega^2 - \alpha^2 > 0$. For this case $b = \alpha/2$, $m^2 + \alpha^2/4 = \Omega^2$, $k_{1,2} = \alpha i/2 \pm \sqrt{(\Omega^2 - \alpha^2/4)}$. We thus have

$$u_z(z,t) = Ue^{-(\alpha/2)z}e^{i(-\omega t \pm z\sqrt{\Omega^2 - \alpha^2/4})} \tag{27a}$$

Case 2: $4\Omega^2 - \alpha^2 = 0$. For this case $k_{1,2} = \alpha i/2$.

$$u_z(z,t) = Ue^{-(\alpha/2)z}e^{-i\omega t} \tag{27b}$$

Case 3: $4\Omega^2 - \alpha^2 < 0$. For this case $k_{1,2} = (\alpha/2 \pm \sqrt{(\alpha^2/4 - \Omega^2)})i$.

$$u_z(z,t) = Ue^{-((\alpha/2)\pm\sqrt{\alpha^2/4 - \Omega^2})z}e^{-i\omega t} \tag{27c}$$

It is observed clearly that only in Case 1 (i.e., $4\,\Omega^2 - \alpha^2 > 0$), can wave propagate along the longitudinal direction of the rod, with decreasing amplitude. We discuss this and other phenomena in the next section.

3. Numerical results

In the numerical example, we consider the FG-MEE rod made of $BaTiO_3$-$CoFe_2O_4$ with variable volume fraction (v_f) of $BaTiO_3$. The material properties of the composite are calculated using the micromechanics approach (Kuo & Pan, 2011; Kuo & Wang, 2012). In what follows, we consider five different material combinations, by taking the volume fraction of $BaTiO_3$ as 0%, 25%, 50%, 75%, and 100%, respectively. Obviously, when $v_f = 0$, the composite is purely piezomagnetic (PM), whilst $v_f = 100\%$ corresponds to a purely piezoelectric (PE) material (Chen, Pan, Wang, & Zhang, 2010). The effective MEE material properties are listed in Table 1.

When $U = 1$, the normalized amplitude $e^{-(\alpha/2)z}$ in Eq. (27b) is shown in Fig. 2 for the rod made of MEE composite (the middle column with 50% MEE in Table 1). It is noted that, on the one hand, the amplitude decreases along the wave propagation direction when time is fixed. On the other hand, the amplitude decreases greatly with increasing gradient index α (in m^{-1}).

The relations between the quantity Ω in Eq. (25) and the wave number k for the three different Cases are shown in Figs. 3–5 for the rod made of MEE composite (the middle column with 50% MEE in Table 1). We first point out that when gradient index $\alpha = 0$ and the FG-MEE coupling factor $C_{\text{mee}} = 0$, our solution reduces exactly to the corresponding purely elastic rod case (Achenbach, 1973), which verifies the formulation derived in this paper. We now take Ω as real and positive, which gives either a complex or a purely imaginary wave number k. In physical terms, purely imaginary and complex wave numbers correspond to the standing wave with decaying amplitudes as z increases. Fig. 3 shows the relationship between Ω and the real part of k for different gradient factor α for Case 1 ($4\Omega^2 - \alpha^2 > 0$). This is the only case where wave propagates along the rod. The curves are hyperbolas with their asymptotes being $\Omega = Re(k)$ (corresponding to $\alpha = 0$). Their focuses are on the vertical axis at $(0, \alpha/\sqrt{2})$, linearly proportional to α. Fig. 4 shows the relationship between Ω and the imaginary part of k for different α for the Cases 1 ($4\Omega^2 - \alpha^2 > 0$) and 2 ($4\Omega^2 - \alpha^2 = 0$). For these cases, $\text{Im}(k) = \alpha/2$. In other words, $Im(k)$ is independent of Ω. Finally, Fig. 5 represents circles with radii $\alpha/2$ for Case 3 ($4\Omega^2 - \alpha^2 < 0$). The curves satisfy the relation of $(b - \alpha/2)^2 + \Omega^2 = \alpha^2/4$ with centers at $(\alpha/2, 0)$.

It is noted that when $\alpha = 0$, $c = \sqrt{\left[\left(B_3^0 - C_{\text{mee}}\right)/\rho^0\right]}$. Thus, the effect of different volume fractions v_f on the phase velocity of the wave, as well as on the effective modulus $B_3^0 - C_{\text{mee}}$ and effective Poisson's ratio ν_{eff} in the rod, can be studied as shown in Table 2. It is observed from Table 2 that the effective Poisson's ratio decreases (from 0.3725 to 0.2906, or decreases about 22%) with increasing volume fraction. Similarly, the PM rod has the largest phase velocity c whilst the PE rod has the smallest

Table 1
Effective material coefficients for the $BaTiO_3$–$CoFe_2O_4$MEE composite rod based on the micromechanics approach (Kuo & Pan, 2011; Kuo & Wang, 2012).

v_f	0% (PM)	25% (MEE)	50% (MEE)	75% (MEE)	100% (PE)
c_{11}^0	286	245	213	187	166
c_{12}^0	173	139	113	93	77
c_{13}^0	170	138	113	93.8	78
c_{33}^0	269.5	235	207	183	162
c_{44}^0	45.3	47.6	49.9	52.1	43
e_{31}^0	0	−1.53	−2.71	−3.64	−4.4
e_{33}^0	0	4.28	8.86	13.66	18.6
e_{15}^0	0	0.05	0.15	0.46	11.6
κ_{11}^0	0.08	0.13	0.24	0.53	11.2
κ_{33}^0	0.093	3.24	6.37	9.49	12.6
μ_{11}^0	5.9	3.57	2.01	0.89	0.05
μ_{33}^0	1.57	1.21	0.839	0.47	0.1
q_{31}^0	580	378	222	100	0
q_{33}^0	700	476	292	136	0
q_{15}^0	550	331.2	185	79	0
d_{11}^0	0	−3.09	−5.23	−6.72	0
d_{33}^0	0	2334.15	2750	1847.49	0
ρ^0	5.3	5.43	5.55	5.66	5.8

Units: elastic constants, c_{ij}^0, in 10^9 N/m^2, piezoelectric constants, e_{ij}^0, in C/m^2, piezomagnetic constants, q_{ij}^0, in N/A m, dielectric constants, κ_{ij}^0, in 10^{-9} C^2/N m^2, magnetic constants, μ_{ij}^0, in 10^{-4} N s^2/C^2, magnetoelectric coefficients d_{ij}^0, in 10^{-12} N s/VC and ρ^0 in 10^3 kg/m^3.

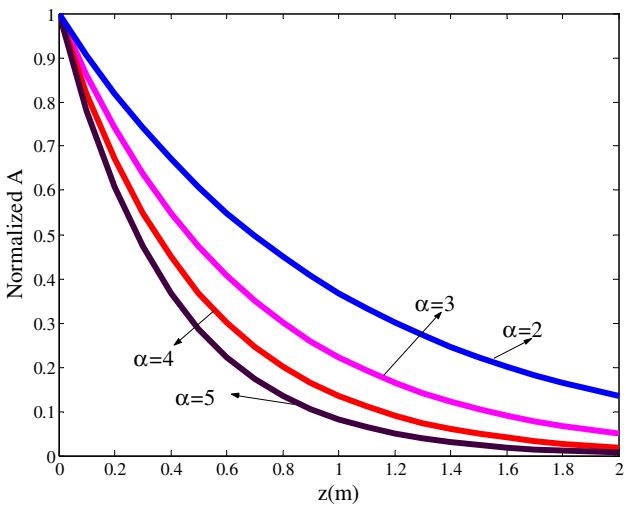

Fig. 2. Variation of the normalized amplitude of the wave u_z along the longitudinal z-direction of the rod made of 50% MEE with different gradient index α (in the unit of m^{-1}) (for Case 2 as given in Eq. (27b)).

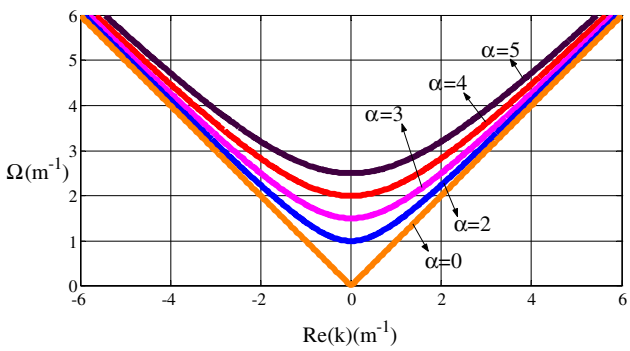

Fig. 3. Variation of Ω vs. $Re(k)$ when $4\Omega^2 - \alpha^2 > 0$.

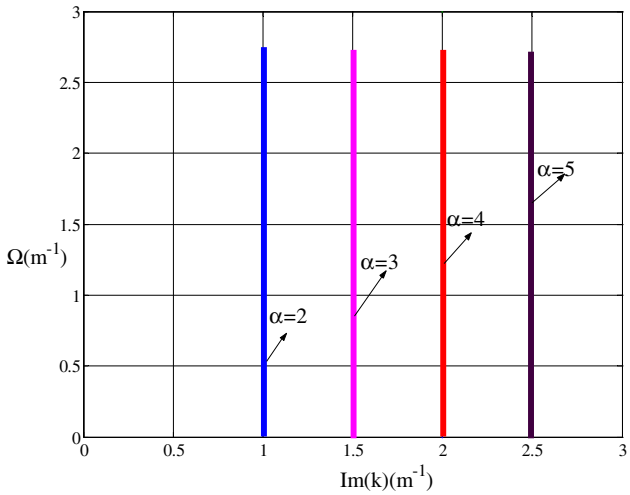

Fig. 4. Variation of Ω vs. $Im(k)$ when $4\Omega^2 - \alpha^2 \geqslant 0$.

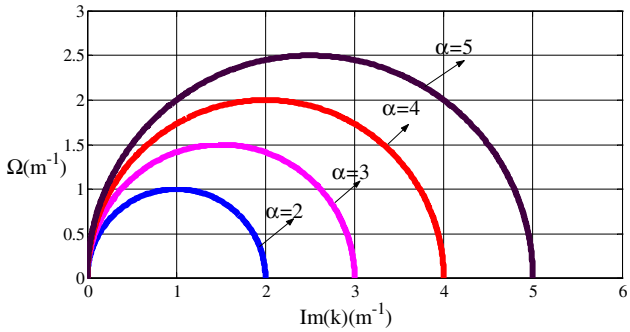

Fig. 5. Variation of Ω vs. $Im(k)$ when $4\Omega^2 - \alpha^2 < 0$.

Table 2
Phase velocity c, effective Young's moduli $B_3^0 - C_{mee}$, effective Poisson's ratio ν_{eff}, and circular frequency ω in PM, MEE and PE rods

v_f	0% (PM)	25% (MEE)	50% (MEE)	75% (MEE)	100% (PE)
c (10^3m/s)	5.2131	5.171	5.1439	5.0947	5.0498
B_3^0 (10^{11} N/m^2)	1.6845	1.5727	1.4705	1. 3595	1.2535
C_{mee} (10^{11} N/m^2)	0.2442	0.1221	0.00199	−0.1135	−0.2255
$B_3^0 - C_{mee}$ (10^{11} N/m^2)	1.4404	1.4506	1.4685	1.473	1.479
ν_{eff}	0.3725	0.3544	0.3339	0.3137	0.2906
C_{mee}/B_3^0 (%)	14.49	7.76	0.14	−8.35	−17.99
$\omega = kc$ (10^{-3} s^{-1})	2.4i	1.9i	1.7i	2.6i	1.8

one. It is also clearly shows that the PE rod has the largest ratio C_{mee}/B_3^0 whilst the MEE rod has the smallest one. These results indicate that the influence of the FG-MEE coupling factor C_{mee} on the effective Young's modulus cannot be ignored for the rod made of PM and PE materials. For the MEE (v_f = 50%) material, however, the coupling can be ignored and one could just treat the MEE rod as a purely elastic one. The last row in Table 2 shows the circular frequency as a function of the volume fraction ratio, which is obtained using Eq. (21a) with R = 0.05 m. It should be noticed that only for the piezoelectric (PE) case, Eq. (21a) has a solution of the real frequency; otherwise, the frequency will be purely imaginary (this character is independent of the value of R). These interesting features should be useful in the optimal design of magnetoelectroelastic transducers based on multifunctionality (i.e., Rubio et al., 2009).

4. Conclusion

We studied the wave features in a functionally graded magneto-electro-elastic rod made of piezoelectric $BaTiO_3$ and piezomagnetic $CoFe_2O_4$. The materials properties are assumed to vary exponentially along the rod direction. By introducing the effective Poisson's ratio, we found that the gradient factor as well as the material coupling can substantially affect the

wave features in the rod. The effective Young's modulus and Poisson's ratio in the composite rod can be also significantly affected by the magneto-electro-elastic coupling factor C_{mee} defined in this paper.

Acknowledgement

The work is supported by National Youth Science Foundation of China (11202190).

References

Achenbach, J. D. (1973). *Wave propagation in elastic solid*. New York: North-Holland.
Bayrashev, A., Robbins, W. P., & Ziaie, B. (2004). Remote low frequency powering of microsystems using piezoelectric-magnetostrictive laminate composites. *Sensors and Actuators A, 114*, 244–249.
Bhangale, R., & Ganesan, N. (2006). Static analysis of simply supported functionally graded and layered magneto-electro-elastic plates. *International Journal of Solids and Structures, 43*, 3230–3253.
Chen, W. Q., Pan, E., Wang, H. M., & Zhang, C. Z. (2010). Theory of indentation on multiferroic composite materials. *Journal of the Mechanics and Physics of Solids, 58*, 1524–1551.
Huang, D. J., Ding, H. J., & Chen, W. Q. (2007). Analytical solution for functionally graded magneto-electro-elastic plane beams. *International Journal of Engineering Science, 45*, 467–485.
Kuo, H. Y., & Pan, E. (2011). Effective magnetoelectric effect in multicoated circular fibrous multiferroic composites. *Journal of Applied Physics, 109*, 104901.
Kuo, H. Y., & Wang, Y. L. (2012). Optimization of magnetoelectricity in multiferroic fibrous composites. *Mechanics of Materials, 50*, 88–99.
Pan, E. (2001). Exact solution for simply supported and multilayered magneto electro elastic plates. *Journal of Applied Mechanics, 68*, 608–618.
Pan, E., & Han, F. (2005). Exact solution for functionally graded and layered magneto-electro-elastic plates. *International Journal of Engineering Science, 43*, 321–339.
Pan, E., & Heyliger, P. R. (2002). Free vibrations of simply supported and multilayered magneto-electro-elastic plates. *Journal of Sound Vibration, 252*, 429–442.
Quek, S. T., & Wang, Q. (2000). On dispersion relations in piezoelectric coupled plate structures. *Smart Materials and Structures, 10*, 859–867.
Rubio, W. M., Silva, E. C. N., & Paulino, G. H. (2009). Toward optimal design of piezoelectric transducers based on multifunctional and smoothly graded hybrid material systems. *Journal of Intelligent Material Systems and Structures, 20*, 1725–1746.
Wang, Q., & Quek, S. T. (2000). On dispersion relations in piezoelectric coupled beams. *AIAA Journal, 38*, 2357–2361.
Wang, Q., & Varadan, V. K. (2002). Longitudinal wave propagation in piezoelectric coupled rods. *Smart Materials and Structures, 11*, 48–54.
Wu, T. L., & Huang, J. H. (2000). Closed form solutions for the magnetoelectric coupling coefficients in fibrous composites with piezoelectric and piezomagnetic phases. *International Journal of Solids and Structures*, 37, 2981–300.
Xue, C. X., Pan, E., & Zhang, S. Y. (2011). Solitary waves in a magneto-electro-elastic circular rod. *Smart Materials and Structures, 20*, 105010.
Yu, J. G., & Wu, B. (2009). Circumferential wave in magneto-electro-elastic functionally graded cylindrical curved plates. *European Journal of Mechanics – A/Solids, 28*, 560–568.
Zhang, C. L., & Chen, W. Q. (2010). Torsional wave propagation in a circumferentially poled piezoelectric cylindrical transducer with unattached electrodes, IEEE Trans. *Ultrasonics Ferroelectrics and Frequency Control, 57*, 1230–1236.
Zhang, S. Y., & Liu, Z. F. (2008). Three kinds of nonlinear dispersive waves in elastic rods with finite deformation. *Applied Mathematics and Mechanics, 29*, 909–917.
Zhao, L., & Chen, W. Q. (2010). Plane analysis for functionally graded magneto-electro-elastic materials via the symplectic framework. *Composite Structures, 92*, 1753–1761.